

Chapter 16

SOLAR RADAR

William A. Coles

Department of Electrical and Computer Engineering, University of California at San Diego

bcoles@ucsd.edu

Abstract

A serious long-term attempt to study the corona using radar was made between 1961 and 1969, but it was unsuccessful because the characteristics of the radar echo could not be explained. In retrospect it was not possible to adequately model the radar echoes because we did not know enough about the corona at that time. Further observations became impossible as radar astronomy evolved and the technique has been almost forgotten. In this chapter we propose to revive the solar radar technique. We discuss the theory, review the early observations, provide a tenable explanation of them, propose new experiments, and outline the likely development of the technique.

1. Introduction

The Sun was the second target attempted in the development of radar astronomy (after the Moon). The first detailed calculations of the expected echo and the radar parameters required were done by Kerr (1952), and echoes were first detected at 25 MHz by a Stanford group in 1959 (Eshleman *et al.* 1960). A dedicated 38 MHz solar radar was built at El Campo, Texas by an MIT group and regular observations were made between 1960 and 1969 (James *et al.* 1970). Unfortunately the observations were not fully understood, and they have not contributed much to our present understanding of the corona. An excellent discussion of solar radar theory and the early observations, is in Chapter 7 of the book *Radar Astronomy* by Evans & Hagfors (James 1968). A more recent review is given by Rodriguez (2000).

In retrospect the early observers faced several insurmountable difficulties. First, the large scale structure of the corona is often dominated by features, such as coronal holes and coronal mass ejections, which were unknown at the time. Second, the microstructure that governs the angular spread of the backscattered

radiation was also unknown. Third, the radar turning point is at the base of the solar wind, which had just been discovered and was largely unknown. Finally, they did not have simultaneous optical observations to help constrain the coronal geometry. Eventually interest in the solar observations waned, the radar was scrapped, and radar astronomy evolved towards the use of higher frequencies. Higher frequencies penetrate through the transition region into the cool dense plasma of the chromosphere where they are heavily attenuated, so it became impossible to repeat the observations and solar radar has been almost forgotten.

It is probable that new radar observations with modern signal processing, dual polarization, and multiple frequencies, combined with modern optical, UV, and X-ray observations, could make a significant contribution to the fundamental questions of coronal heating and solar wind acceleration. Solar radar observations near 50 MHz are possible at present with at least two radars, the Jicamarca ionospheric radar in Peru and the Gadanki atmospheric radar in India. It may soon be possible to observe between 18 and 26 MHz using a new ionospheric heater planned for the Arecibo observatory. The radar echos from Gadanki could be imaged with the GMRT radio telescope, and both Arecibo and Jicamarca echos could be imaged with the proposed LOFAR array. So prospects for revival of solar radar are encouraging.¹

2. Theory

The propagation constant $k = n\omega/c = \beta + j\alpha$ for a radio wave in a warm plasma, such as the corona, depends on the density, magnetic field, and electron temperature. A normally incident radar wave is reflected at the height H at which β becomes zero. This depends only on the density and the magnetic field. The loss term α depends on the collision frequency and thus T_e as well. To the accuracy necessary here, the refractive index is given by $n^2 = 1 - \omega_p^2/\omega(\omega \pm \omega_{ce})$, where $\omega_p^2 = n_e e^2/m_e \epsilon_0$ gives the electron plasma frequency, and $\omega_{ce} = eB/m_e c$ is the electron cyclotron frequency. The refractive index $n < 1$ so the phase velocity $V_p = c/n > c$, but the wave is highly dispersive and the group velocity $V_g = d\omega/dk = nc < c$. The power loss term $2\alpha = \nu(1 - n^2)/(nc)$, where ν is the collision frequency. In the corona $\nu = 1.81 \times 10^{-6} n_e A_1(2)/T_e^{1.5}$ where $A_1(2) = \ln(1 + (10^7 4kT_e/c^2 e^2 n_e^{0.333})^2)$. The two-way delay T_d and optical depth τ are determined by the integrals given below.

$$T_d = 2 \int_{Earth}^H ds/V_g \quad \text{and} \quad \tau = \int_{Earth}^H 2\alpha ds. \quad (16.1)$$

¹Note added in proof: A series of new 50 MHz observations has been made at Jicamarca by Coles *et al.* (2004) using the same modulation and pulse width as El Campo. These observations have not shown any valid echos. This negative result suggests that the echo amplitude may have been significantly overestimated and makes prospects for revival of solar radar less encouraging than when the chapter was written.

We have used these expressions, with estimates of the density and temperature in the coronal holes and the equatorial streamers, to obtain the reflection height H , delay T_d , and loss $\exp(2\tau)$ for the two circular polarizations vs. frequency. The density models and the height of the turning points are shown in Figure 16.1. The coronal hole density is from Guhathakurta *et al.* (1999), and the streamer density is from Parenti *et al.* (2000). The kinetic temperature of the electrons is not as well known, so we used rough values of $T_e = 1 \times 10^6 K$ in the coronal holes and $T_e = 2 \times 10^6 K$ in the streamers. The magnetic field is even less well known. We assumed that it was the same in the coronal holes and streamers and extrapolated inwards using $B_r \propto R^{-2}$. This undoubtedly underestimates the field. The left-handed mode (LH) has smaller refractive index change than the RH mode so it turns deeper in the corona (increasing the delay). Likewise the coronal hole plasma is less dense so the reflection points are deeper than in the equatorial plasma.

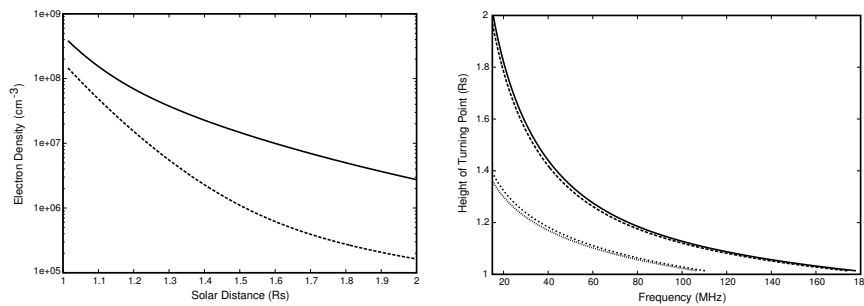


Figure 16.1. Plasma density versus solar distance (left panel) and reflection height versus frequency (right panel). Two plasma models, corresponding to streamers with $T_e = 2 \times 10^6 K$ and coronal holes with $T_e = 1 \times 10^6 K$ are given. The upper traces are from the streamer model in both panels. The magnetic field is the same in both. The free space delay is $4.64 \text{ s}/R_\odot$.

The total path-integrated contribution of the plasma to the delay is the almost same for both polarizations. Thus the differential delay between the polarizations ($\approx 150 \text{ ms}$ at 38 MHz) is almost entirely due to the different height of the turning points. The delays can be measured with sufficient accuracy to provide good estimates of both the density and the magnetic field near the turning points. Since the density is already reasonably well-known from optical observations, the most important result will be the magnetic field estimate.

The loss increases dramatically if the wave “punches through” the corona into the transition region where the temperature decreases and the density increases. This will probably occur near 110 MHz in the coronal holes and 180 MHz in the streamers but we do not have sufficient information to model the effect. The lower frequency limit, $\sim 15 \text{ MHz}$, is set by the ionospheric cutoff, but

increasing noise, refraction and scintillation will make operation down near the cutoff unattractive. The plasma delay and the signal loss are shown in Figure 16.2. The loss is higher in the coronal holes because the temperature is lower and the collision frequency is higher, however the plasma delay is lower because the turning point is nearer the Sun where the density gradient is higher.

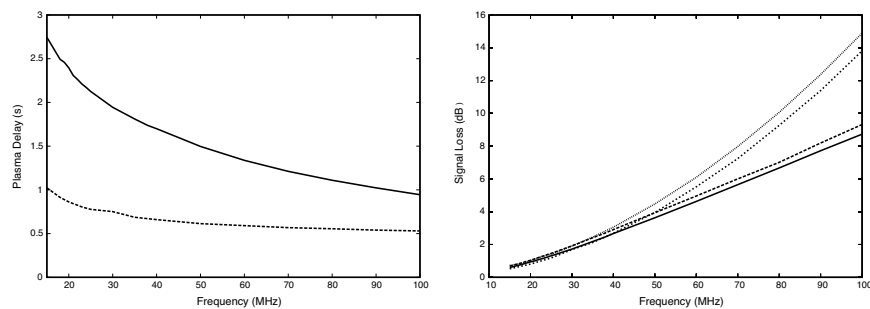


Figure 16.2. Plasma delay versus frequency (left panel) and loss versus frequency (right panel) for the models given in Figure 16.1. The coronal hole model gives less plasma delay and more loss.

The effect on delay of a step density increase, such as would occur during a fast Earthward CME, is plotted in Figure 16.3. When the step passes the turning point it carries the turning point outward, reducing the free space delay abruptly. When both polarizations reflect from the edge of the step the differential delay is entirely due to the differential plasma contribution so the sense of the difference is reversed. When the step moves far enough outward the turning points of the two polarizations separate again and the differential delay changes back to the normal sense. The total delay then increases slowly as the remainder of the line of sight fills with denser plasma.

The returned echo will be scattered into a Doppler spectrum by motion of the plasma at the turning point. The Doppler spectrum will be shifted by the velocity of the solar wind and broadened by the random thermal and wave motions in the plasma. The reflection process is an electron resonance but it is a collective effect of many electrons. In this case the broadening is not due to the thermal velocity of the electrons but to that of the ions. This phenomenon has been studied in the case of Bragg backscattering in the ionosphere (Vanzandt & Bowles 1960; Fejer 1960), but does not appear to have been studied in the case of coherent reflections such as solar echoes.

Radars normally transmit and receive with the same antenna, and the antenna beam illuminates the entire target. The antenna area A and gain G are related by $G = 4\pi A/\lambda^2$. In this case we can calculate the received power in terms of

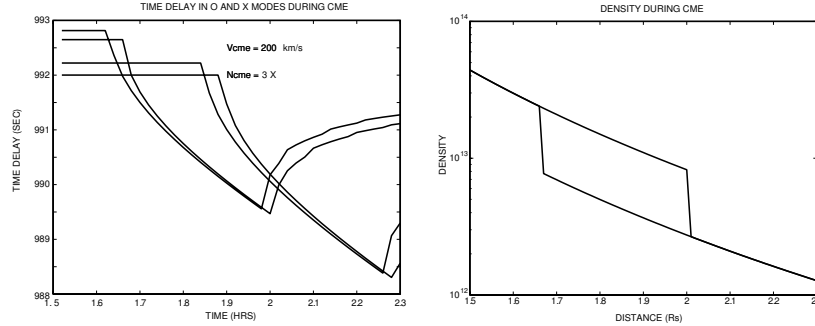


Figure 16.3. Simulation of a spherically symmetric density step of three times the background density, moving outwards at 200 km/s = $1R_{\odot}/h$. The delays are shown for RH and LH polarizations at 18 and 26 MHz. The density profile is shown at 1.68 h and 2.0 h.

the target cross-section σ , which is the area of the equivalent isotropic reflector. (The radar cross section of a large sphere is equal to its cross sectional area, regardless of the surface roughness.) The transmitted flux is $S_t = P_t G / 4\pi R^2$. The reflected power $S_t \sigma$ is reradiated isotropically, so the total returned power at the antenna is

$$P_r = P_t \sigma \frac{GA}{(4\pi R^2)^2} = P_t \sigma \frac{A^2}{4\pi \lambda^2 R^4}. \quad (16.2)$$

The reflected power is further reduced by the loss due to propagation through warm plasma as discussed earlier. The returned signal is weak, because the gain of the transmitting antenna is low at the low frequencies necessary to obtain a coronal reflection, so the antennas must be physically large. This means that the noise for all practical antennas will be dominated by solar noise. Thus we can calculate the signal to noise ratio directly from the solar flux $S_s = 2kT_e \Omega_s B / \lambda^2$ W/m². Here B is the bandwidth and $\Omega_s = \pi(R_{\odot}/R)^2$ is the solid angle subtended by the Sun. The resulting signal to noise ratio is

$$\frac{P_r}{P_s} = \frac{P_t A}{8\pi k T B R^2}. \quad (16.3)$$

It is interesting that the signal to noise ratio (except for plasma loss) is independent of frequency. This is because both the solar noise and the antenna gain increase with frequency at the same rate.

If the reflecting surface were a smooth sphere the echo would come entirely from a small region in the center of the apparent disk called the specular reflection. The cross section of such a reflection is $\sigma = \pi R_c^2$, where R_c is the radius of the reflecting surface. The actual area contributing to the specular reflection would be roughly that of the first Fresnel zone $\approx \pi R_c \lambda / 2$.

If the reflecting surface is rough on a small scale, the wave will be backscattered into an angular spectrum of width θ_{rms} . Each specular reflection will be broadened into a patch of diameter $\approx \theta_{rms}R_c$. If the surface is very rough, such as the surfaces of the terrestrial planets, moons, and asteroids, the echo will be distributed more or less uniformly over the half of the reflecting surface that faces the radar.

To determine the backscattering angular spectrum for the corona one must characterize the surface roughness to obtain an estimate of the rms gradients of the surface. The density fluctuations can be described by their structure function $D_{ne}(\mathbf{s}) = \langle (n_e(\mathbf{r}) - n_e(\mathbf{r} + \mathbf{s}))^2 \rangle$, so the rms density gradient on a scale s is given by $\delta n_e/s = D_{ne}^{0.5}(s)/s$. The structure function $D_{ne}(s)$ is power law in nature but the exponent changes at the inner scale $s = \ell_i$. At scales $s < \ell_i$, $D_{ne}(s) \propto s^2$ so $\delta n_e/s$ is independent of s . At scales $s > \ell_i$, $D_{ne}(s) \propto s^\alpha$ where $\alpha < 2$, so $\delta n_e/s$ drops with increasing scale s . We have measurements of $D_{ne}(s)$ near $s = \ell_i$ from radio scattering observations and we can use a recent model (Armstrong *et al.* 2000) to obtain a lower bound at a typical radar turning point of $1.4R_\odot$. At that distance the model gives $D_{ne}(s < \ell_i) \geq 2.1 \times 10^{-6} n_e^2 (s/\ell_i)^2$ and $\ell_i \approx 1040$ m.

The gradient of the reflecting surface can be obtained by translating the density fluctuation δn_e into a height fluctuation $\delta H = \delta n_e / (dn_e/dR)$ where dn_e/dR is the radial gradient. The rms surface gradient is then $dH/dR = (D_{ne}^{0.5}(\ell_i)/\ell_i) / (dn_e/dR)$. The density gradient at $1.4R_\odot$ is $dn_e/dR \approx n_e/6R$ so $dH/dR \approx 220$! The effect of anisotropy will increase this by about an order of magnitude, but it is very large in any case. The coronal reflecting surface is very different from other targets in the solar system. It is smooth on scales smaller than the inner scale, which is about 100 times larger than the wavelength. However the surface gradients are extremely large. It appears that the incident wave will be backscattered into a very wide angular spectrum by reflection from a violently undulating smooth surface, rather than a rough surface.

To help visualize the nature of the reflecting surface we show simulated one-dimensional cuts $n_e(r)$ in the radial and tangential directions in Figure 16.4. The Fourier transform of $n_e(r)$ was generated from a sampled gaussian random process and scaled so its squared magnitude matches the anisotropic spectrum measured by radio scattering near the Sun (Grall *et al.* 1997). It was then Fourier transformed back and the mean radial gradient was added. The fluctuations in $n_e(r)$ are normalized to the mean value of the simulation. The two-dimensional spectra at this distance have an axial ratio of about 50, so the two cuts have very different spatial scales. The smallest scales in the tangential direction are about 1 km, whereas in the radial direction they are about 50 km. The reflecting surface will be at the rising edge of one of these radial bumps. It will be carried outward until the peak density drops below the critical value, then it will jump

back to the following bump. If these density bumps are convected with the plasma flow (velocity V_f), then the mean Doppler shift will be $\Delta\nu = 2V_f\nu/c$, however they could be traveling density waves (wave velocity V_w), which would increase the Doppler shift to $\Delta\nu = 2(V_f + V_w)\nu/c$.

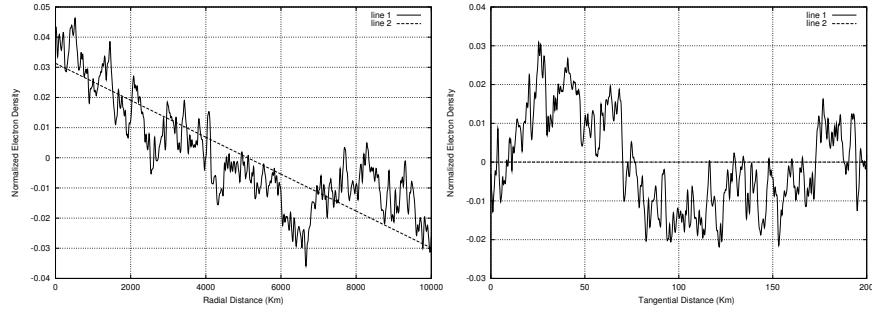


Figure 16.4. Simulation of n_e vs radial distance (left panel), and n_e vs tangential distance (right panel). The mean radial gradient is shown as a dashed line in the left panel.

The radial gradients of the fluctuations are very much larger than the mean radial gradient. Thus the height of the reflecting surface will vary by 1000's of km as these structures move outward. The structure of the reflecting surface is illustrated in Figure 16.5, which is a two-dimensional cut through the equatorial plane. The region where the wave can propagate is white, where the wave is cutoff it is black. The wave is incident from the right and is reflected by the black structure. However, in order to display the plot conveniently we increased the radial gradient by a factor of 20. Thus the highly filamentary radial structures in Figure 16.5, should actually be even more elongated. This is an unusual type of reflecting surface which apparently has not been studied before. It seems likely that it will scatter the incident wave into a wide angular spectrum, but it is also possible that multiple reflections in the low density channels will greatly increase the loss in the manner of an optical beam trap. Study of the cross polarized echo may be useful here. Evidently some analysis and perhaps simulation of this situation will be necessary.

The corona has a great deal of large-scale structure controlled by the coronal magnetic field. The gradients in such structures are small compared with the turbulent gradients, but the changes in the mean density and temperature are significant. Near solar maximum the height of the reflecting surface at 38 MHz will be about $1.4 R_\odot$ so the radar cross section will be about $\sigma = 2\pi R_\odot^2$. Near solar minimum the large scale structure is characterized by a high density equatorial streamer belt and coronal holes over both poles. The height of the reflecting surface will be about $1.4 R_\odot$ over the streamer belt and $1.2 R_\odot$ over the polar holes. The polar hole echo is weaker, as shown in Figure 16.2, so

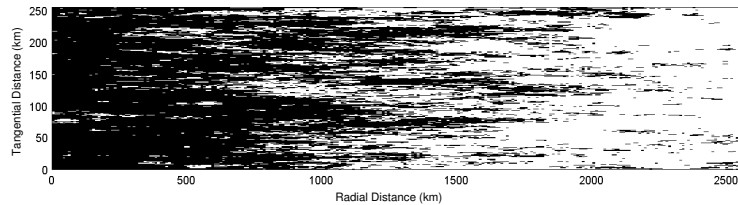


Figure 16.5. Simulation of n_e in the equatorial plane. In the dark regions the wave frequency is above the plasma frequency and the wave cannot propagate. The wave is incident from the left and reflects from the black structures. The pixel size is 1 km by 10 km. The radial gradient has been increased by a factor of 20 to keep the plot on a convenient scale.

the average cross section at solar minimum will be about half that at solar maximum.

At all phases of the solar cycle coronal mass ejections (CMEs) are common, although the rate is higher at solar maximum and during the declining phase of solar activity. CMEs often have a roughly spherical geometry comparable in size with the solar disk. However, they are far from a smooth sphere and many irregular events occur. One of the simplest large CMEs observed with LASCO is shown in Figure 16.6 below. Such a CME would have a stronger echo than the background corona because it will not only increase the area, it will push the reflecting surface out and reduce the loss.

We have considered only the total reflection that occurs at the location where the refractive index goes to zero. The wave can also be reflected from periodic density fluctuations that satisfy the Bragg condition. The density fluctuations can be thermal fluctuations or MHD waves. In either case, only a small amount of the incident power will be reflected at any distance, so the echo is distributed over range. This is a very useful phenomenon in the ionosphere but Bragg reflections from the corona are too weak to be measurable with an Earth-based radar.

3. Other Coronal Observations

Solar observations, by any method, are complex and difficult to interpret because there is a large range of spatial structure; the Sun is not constant; and the observations inevitably average over some finite region. It will be essential to interpret solar radar observations in conjunction with other coronal observations. Here we outline the other coronal data that are most likely to be useful in this regard. These include: (1) white light observations of Thomson scattered solar radiation; (2) radio forward-scattering observations; (3) UV

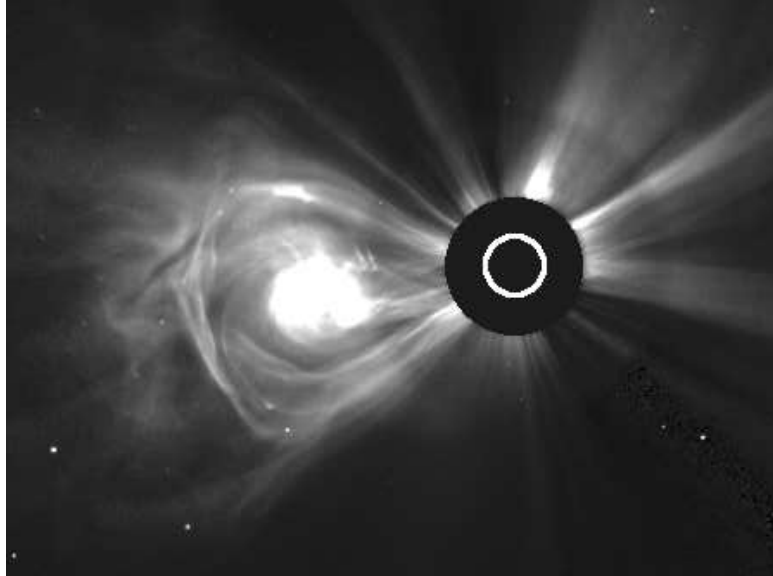


Figure 16.6. A relatively simple large CME known as “the lightbulb” as observed by LASCO C2 and C3. This CME was directed to the north and has been rotated east for convenience. The SOHO/LASCO data are produced by a consortium of the Naval Research Laboratory (USA), Max-Planck-Institut fuer Aeronomie (Germany), Laboratoire d’Astronomie (France), and the University of Birmingham (UK). SOHO is a project of international cooperation between ESA and NASA.

emission line observations; (4) soft X-ray continuum observations; (5) radio emission observations. All of these observations involve important line of sight integrations, and the effect of this is different for each observation. It is usually less severe for observations made on the disk than for observations made off the limbs.

The white light observations are made off the limbs where the direct solar radiation can be blocked with occulting disks. They provide an image of the path integrated coronal electron density. These are the best measurements of large-scale coronal structures such as streamers, coronal holes, and CMEs. An example of a CME observation is shown in Figure 16.6. No existing space-born coronagraph can reach the turning point of feasible solar radars because the occulting disks are too large. Fortunately, the new COR1 coronagraph of the SECCHI instrument on STEREO will reach $1.4 R_{\odot}$. The velocity of well-defined structures like CMEs can be measured by tracking the motion of the feature over time. Smaller structures in streamers have also been tracked, but it has not been possible to measure the velocity in coronal holes by this method because no distinct features can be tracked. White light observations

are not directly sensitive to the magnetic field, but lines of enhanced brightness appear to follow magnetic field lines, and they are believed to be a tracer of the magnetic field.

Radio forward-scattering measurements are also limb observations sensitive to density or density fluctuations. One can, in principle, measure Faraday rotation and thus the magnetic field. However, in the normal limb observation the mean Faraday rotation cancels out and only fluctuations can be observed. If a coherent source, such as a space-craft transponder or a pulsar, is available one can measure the column density. Otherwise one can measure the density fluctuations. These measurements can be very precise but only in the direction of the radio source. In this respect they are complementary to the white light observations, which provide an image but less precision. Radio scattering measurements can measure the micro-turbulence and also the velocity of the microstructure. However the microstructure might be moving with respect to the mean flow, if the density fluctuations are caused by traveling waves, and this potential bias can be very important in the sub-Alfvénic flow near the Sun. The primary value of radio scattering measurements for solar radar is that they can be used to estimate the small-scale density gradients, which determine the angular spread of the radar echo.

Soft X-ray observations can be made both on disk and off the limbs. The emission is free-free bremsstrahlung and the characteristic temperature of the radiating electrons is about 7×10^6 K. This is far above the kinetic temperatures of $1 - 2 \times 10^6$ K, so the soft X-ray emission is really a measure of the high-speed tail of the electron velocity distribution. Such superheating of electrons occurs when they are trapped on closed field lines. Absence of soft X-ray emission is a clear signal of open field lines and this is how coronal holes, which are characterized primarily by open field lines, were discovered.

Ultraviolet emission lines can be observed both on disk and off the limbs. They are sensitive to density, temperature and composition. A great deal of information can be derived from these observations but very careful modeling is required. They are particularly valuable in the transition region where one can trace the temperature by observation of different ionization states. There is great potential for comparing details of the radar echoes with TRACE and UVCS observations.

Meter wavelength radio emissions have been observed since the dawn of radio astronomy, because the Sun is a very strong radio source at low frequencies. Continuous thermal emission comes from the hot plasma above the reflection point. However, strong transient emissions occur at the local plasma frequency or its harmonics. They are caused by a disturbance, such as a shock or a stream of relativistic electrons. By observing emission at different frequencies one can measure the local density and trace the disturbance outward (and occasionally inward). These local emissions are often much stronger than the thermal

emission from the entire Sun. They can be observed with spectrometers, which average over the entire Sun. However one can also image the emission with a radio-heliograph, which allows one to separate emissions in position, and to compare with other imaging observations. These observations are primarily traces of solar activity and have not been as useful in outlining the quiet regions. They may prove very useful in comparisons with radar echoes.

4. Previous Radar Measurements

The first radar echoes from the Sun were detected by in 1959 (Eshleman *et al.* 1960). They transmitted 40 kW at 25.6 MHz using an antenna with 3450 m² collecting area. The detection was marginally significant in an integration time of 18 min. Regular measurements were made from 1961 to 1969 with a much more powerful system (James *et al.* 1970). They transmitted 500 kW at 38 MHz using an antenna with 20,000 m² collecting area. The signal was much weaker than had been expected on the basis of the 1959 detection—less than one would expect of a spherically symmetric Sun. The only other apparent radar detection was made at 40 MHz using Arecibo in 1965 (Campbell, private communication, 2001). Solar observations at Arecibo were not continued. Attempts to detect a Raman scattered echo at 2380 MHz with the Arecibo radar were unsuccessful (Fitze & Benz 1981).

The El Campo antenna was a manually-phased array with a rather narrow bandwidth. It was steered in declination by changing the length of the transmission lines. The beam width was 8° E-W by 2° N-S, which is enough to transmit for 18 min, then receive for 18 min, once a day. The antenna declination was changed every few days to track the seasonal change in solar declination. The transmitter was frequency-shift (FSK) modulated between frequencies separated by 8 kHz because it was originally thought that the Doppler shift would not exceed this value. However it was increased in subsequent years to 16, 40, and finally 60 kHz. Even 60 kHz, which corresponds to 237 km/s, was not always sufficient and some of the data show evidence of aliasing in the form of negative echo power. Although part of the antenna had two polarizations, measurements of cross polarization were not reported. The signal processing was done with repeated passes of an analog tape through an analog filter bank. The design and operation of this radar was a tour de force with the technology of the day.

The results were a surprise in many respects. The mean delay was close to the expected value, but echoes were received much earlier and much later than the mean. A long-term average of the delay distribution (James 1968) is shown in Figure 16.7. The observations confirmed that the mean electron density used to model the observations was reasonably accurate, which was not surprising since the density model used (Pottasch 1960) was the result of a great many

optical observations. The early echoes must arise from high density structures near the center of the disk. These could come from equatorial streamers but much stronger echoes would come from Earth-directed fast CMEs, which would carry the reflecting surface further outward than normal. The late echoes must have come from the limbs. They could be either high inclination streamers or CMEs on the limb.

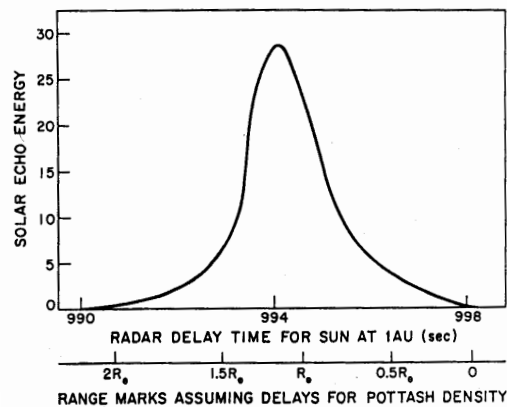


Figure 16.7. Average range distribution of echoes observed with El Campo radar.

The echo strength was weaker than expected and was also highly variable. The annual averages (James 1970), shown in Figure 16.8 are clearly correlated with solar activity. The observations were started as solar activity was declining and the mean echo strength continued to decline with solar activity. It began to increase in 1968 as the solar activity picked up, but the observations were stopped before solar activity reached maximum. This behavior is evidently caused by the reduced cross-section of the polar coronal holes that form at solar minimum as discussed earlier.

The echo strength was also more variable than expected, with daily variations sometimes exceeding a factor of 10. This is apparent in several years of daily observations (James 1968) as shown in Figure 16.9. Some of the unusually large echoes are probably due to large fast CMEs. Those directed toward the Earth will have strong echoes and short delays. Limb CMEs will also show enhanced echoes but longer delays. Other large echoes will occur when a highly inclined streamer is near the limb, and these will also show longer delays.

The most informative displays are the range-Doppler spectra, some of which are shown in Figure 16.10. These were selected from those with high echo amplitude at normal or higher heights (James 1968), which suggests that they

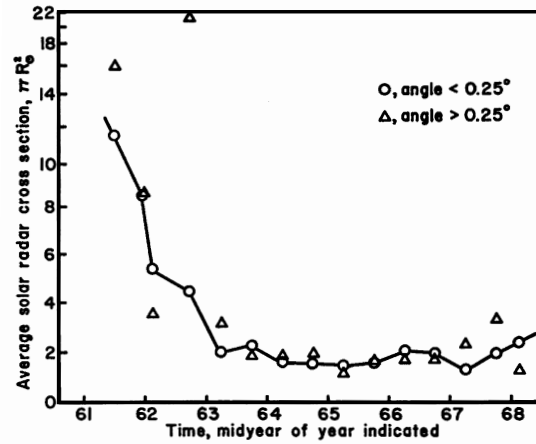


Figure 16.8. Annual average echo strength.

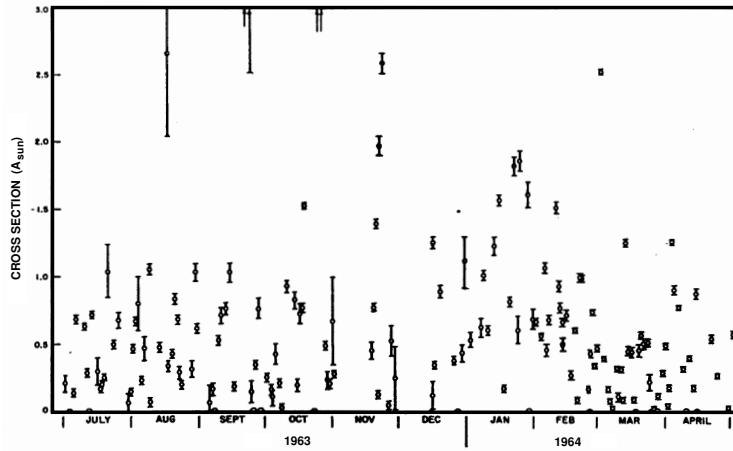


Figure 16.9. Daily measurements of echo strength.

are Earth-directed fast CMEs. The spectra all show a large Doppler broadening corresponding to rms radial velocities of about 100 km/s, consistent with ion temperatures of the order of 2×10^6 K. The spectra clearly shift to the right with elevation, which is consistent with an acceleration. However the echoes

from lower ranges are probably from the flanks of the CME where the velocity is not directed toward Earth. This would cause an apparent acceleration. The mean shift of the higher echoes, of the order of 50 to 100 km/s, is probably a good measure of the radial velocity and is consistent with measurements of fast CME at these heights. These spectra provide some guidance for planning future observations. The Doppler resolution of 5 kHz is sufficient but the finer range resolution would be useful.

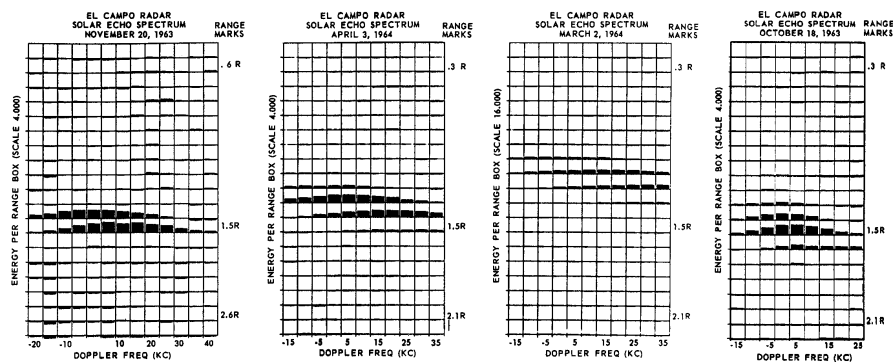


Figure 16.10. Range-Doppler spectra of selected strong echoes. At 38 MHz a velocity of 4 km/s gives a Doppler shift of 1 kHz, so the 5 kHz grid corresponds to 20 km/s.

More typical spectra, such as those in Figure 16.11, show a rich variety of structure (James, 1968). Some features in Figure 16.11 show much less broadening and the broadening is not as smooth as in Figure 16.10. Evidently this must be cool material extending into the corona. Chromospheric material with a kinetic temperature of 10^4 K would have a thermal velocity of about 10 km/s and a Doppler broadening of about 2.5 kHz. Such cool features should be observable in H_α which is regularly monitored on the disk. These spectra suggest that it would be valuable to have finer Doppler resolution, perhaps 1 kHz, in future observations.

5. New Observations

There are a few ionospheric and atmospheric radars which could observe echoes from the Sun with sensitivity comparable with that of El Campo. New radars will have to use pulse amplitude modulation PAM which only provides a maximum 50% duty cycle, because we now know that potential Doppler shifts can exceed the maximum possible FSK shift. It may be possible to use polarization modulation if the cross polarization of the echo is very small. Since

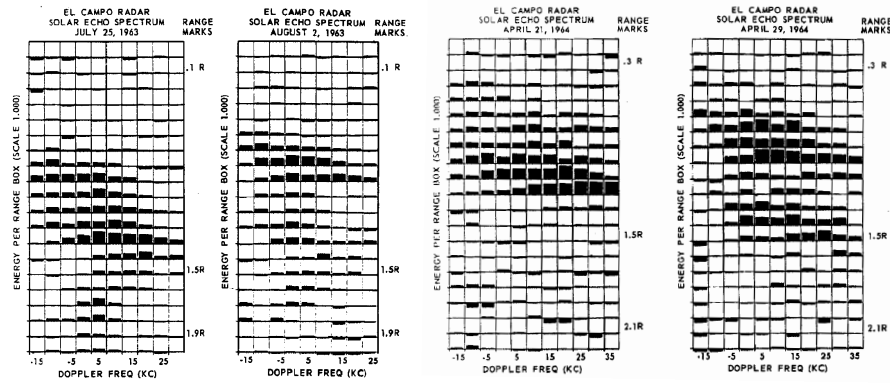


Figure 16.11. Typical Range-Doppler spectra. Notable on these plots are multiple clusters in range and some rather narrow Doppler features. The narrowest features on these spectra could be chromospheric material.

the coherence time of the corona is less than the range resolution, the range decoding must be done incoherently. Thus the effective transmitting power is the peak power P_{pk} times the square root of the duty cycle D . Thus a figure of merit is $F_m = P_{pk}A(DN_p)^{0.5}$, where N_p is the number of polarizations. The echo is probably unpolarized so the signal to noise ratio increases by $\sqrt{2}$ if both polarizations can be measured.

The signal to noise ratio also depends on the pulse width T_p . If the pulse width of the radar is much smaller than the intrinsic width of the echo T_s , the signal to noise ratio decreases as $(T_p/T_s)^{0.5}$. If the intrinsic pulse width exceeds the pulse repetition rate of T_p/D , then it is better to operate in a CW mode where the effective power is P_{avg} but the pulse can be matched to the echo. Estimated values of F_m are given in Table 16.1 for pulse lengths of 2 ms and 500 ms, for existing and potential radars. These have been corrected for the expected signal loss for the streamer model in Figure 16.2 and referenced to El Campo.

The signal to noise ratio does not depend on the frequency resolution because frequency smoothing can be applied either before or after range decoding. Most of the El Campo data were taken with $T_p = 500$ ms and a frequency resolution of 5 kHz. The data may have finer structure in both range and Doppler, so higher resolution in both coordinates would be useful.

The most sensitive existing radar for solar observation is the 50 MHz radar at Jicamarca in Peru. However its maximum pulse width is only 2 ms and the duty cycle is 5%. So if the intrinsic pulse width exceeds 40 ms it should be operated in CW mode. Like El Campo, Jicamarca is a transit instrument that can be steered manually $\pm 3.5^\circ$ from the zenith in either direction. It is bigger than El Campo,

Table 16.1. Comparison of Solar Radar Parameters.

Parameter	Arecibo	Jicamarca	El Campo	NMRF
Frequency (MHz)	15-26	50	38	53
Peak Power (MW)	2.4	2.25	0.5	2.5
Avg Power (kW)	600	112	500	60
Area (1000 m ²)	30	63	20	10
Sensitivity F_m (2ms)	6.7	3.4	-	0.4
Sensitivity F_m (500ms)	2.4	0.5	1	0.04

and it also has dual polarization. However the Jicamarca beam is less than 1° in diameter, so if it were pointed at the Sun to transmit, it would be pointing off the Sun by the time the echo returned. Fortunately the antenna can be separated into sub-arrays and it is possible to use separate sub-arrays for transmitting and receiving. Even with the antenna split Jicamarca has higher sensitivity than El Campo, so solar observations appear to be feasible. Jicamarca is at -7° latitude, so the Sun is within the steering range during two 13-day periods—Oct. 19 to 31; and Feb. 11 to 23. The daily declination change is about $1.6 R_\odot/\text{day}$, so the Sun can only be observed for a few days without repointing the beam. An unsuccessful attempt to observe the Sun with Jicamarca was made in the early 1960's (Bowles, private communication, 2002). This is puzzling because Jicamarca made the first detection of echoes from Venus about the same time, and the Venus detection appears to be more difficult.

Jicamarca is probably best configured with most of the array devoted to transmitting, and only a few modules used for the receiver. However only three of the four original transmitters are presently operational, so it is presently optimal to use three quadrants for transmitting and one for receiving. The transmitters are presently operated at about 75% of their original rating, so the sensitivity is less than that available in the 1960s. The modular nature of Jicamarca allows the use of interferometry to obtain some spatial resolution.

The 53 MHz National MST radar facility (NMRF) at Gadanki near Bangalore in India is another possibility. It has a peak power of 2.5 MW with a duty cycle of 2.5%, and dual polarization. Although it is considerably less sensitive than Jicamarca, it might be possible to use the ‘‘Giant Meter Wavelength Radiotelescope’’ GMRT near Pune as an imaging receiver. With GMRT the sensitivity would not increase, but imaging the echo would be so valuable that this possibility should be explored.

It may soon be possible to use Arecibo as a solar radar. It is likely that a proposed ionospheric heater will be constructed in the next few years, and this heater can be used as a solar radar with minor modifications. The design of

the proposed heater is not complete at this time, but the primary features are becoming clear. The transmitter will operate from 3.0 MHz to 26 MHz. It will have a peak power of about 2.4 MW with a 25% maximum duty cycle, and it will probably be connected to a fixed-feed in the 305 m primary reflector. This will be a very sensitive and flexible system because of the high average power. The heating feed or feeds will only operate up to 9 MHz, so a new high-power feed will have to be constructed for the 18 to 26 MHz band. However we can use an existing dual-polarization 25 MHz receiving-feed mounted on carriage house 2. The beam width would be more than twice that of Jicamarca so there is little possibility of separating the echos from the limbs without an additional receiving antenna.

If the transmitter feed is fixed, then the transmit time will be 18 min, but if the transmitting feed were also mounted on carriage house 2 the total observation time could be increased to 2 h. This would be a real advantage for observing transient events like CMEs. It is feasible to route the transmitter power to the carriage house using an existing high power coaxial-line which is presently unused. This would also simplify the setup considerably and make it much easier to interleave solar observations with other uses of the telescope.

The Arecibo system would have several advantages over Jicamarca: the antenna can be pointed at the Sun any time between March 22 and September 22; the observing time per day is longer; any frequency from 18 to 26 MHz can be used; and sensitivity is better. However observations at Jicamarca will remain interesting because the frequency is different, and the angular resolution is significant.

The analysis of single-antenna data will remain complex because the echo is integrated over the entire Sun. The reflecting surface will have to be located by model fitting, which will have to include correlative optical, UV, and soft X-ray data to constrain the large scale geometry. However some geometries will be unambiguous, for example that of a fast Earth-directed CME. Such a case will be particularly valuable in measuring the pre-CME corona, because the incident wave will be reflected at the leading edge of the density compression. The CME will act as a test reflector moving out through the pre-existing corona. The location of cool filaments may also be unambiguous as they can be observed on the disk with an H_{α} monitor.

6. Use of an Imaging Receiver

The most serious weaknesses of the single antenna radars: (1) the ambiguity in the location of the reflections and the resulting complexity in echo analysis; (2) the limited frequency range and thus height coverage; (3) limited tracking time. The ambiguity problem could be eliminated by receiving the echo with an imaging array capable of spatially resolving the coronal features of interest.

Such an array would provide a range-Doppler spectrum for each beam, mapping the reflecting surface in velocity, density, and magnetic field. This would be possible using the NMRF and GMRT in India, although the planned 53 MHz receiver at GMRT has not yet been implemented. Another possibility is the LOFAR array, now being designed primarily for radio astronomy. LOFAR would be ideal for receiving the solar echo (provided it is located reasonably close to the transmitter) because it is designed to have a good instantaneous beam shape. Most imaging arrays, including GMRT, have rather high sidelobes on their “instantaneous beam.” They synthesize a clean beam by Earth-rotation averaging, which typically takes at least half a day. A LOFAR array in the south-west USA could work with both Arecibo and Jicamarca transmitters. Unfortunately Arecibo and Jicamarca cannot point at the Sun at the same time because Arecibo cannot point south of 0° declination and Jicamarca cannot point north of -5° declination.

The LOFAR goal is to have the instantaneous beam sidelobes $< 0.5\%$ of the peak so the dynamic range of the map could exceed 100. Since the signal to noise ratio is limited by the transmitter flux, rather than the sensitivity of the receiver, it is unlikely that LOFAR could reach a dynamic range of 100 with existing transmitters. Even if the sidelobe levels are somewhat higher LOFAR should be able to produce excellent maps of the reflecting surface. The GMRT/NMRF combination cannot provide the high spatial resolution and high dynamic range of LOFAR, but it would be capable of resolving the major coronal features of interest, i.e. coronal holes, CMEs, streamers, etc. Furthermore a 53 MHz system at GMRT could be ready long before LOFAR, so serious consideration should be given to NMRF. The main uncertainty appears to be the coronal loss at 50 MHz. This could be resolved by observations at Jicamarca which would help judge the feasibility of NMRF/GMRT observations.

Acknowledgments

The author wishes to thank Barney Rickett, Mike Sulzer, John Harmon, Brett Isham, Don Campbell, Ernie Hildner, Mukul Kundu, Ken Bowles, and Jesse James for helpful comments, suggestions, and discussions.

References

- Armstrong, J. W., W. A. Coles, & B. J. Rickett, 2000, *JGR*105, 5149
- Coles, W. A., Sulzer, M. P., Harmon, J. K., Chau J. L. & Woodman R. F. 2004, presented at "Ionospheric Interactions Workshop," Santa Fe, NM, 2004 April 18-21
- Eshleman, V. R., R. C. Barthle, & P. B. Gallagher, 1960, *Science*, 131, 329
- Fejer, J.A., 1960, *JGR*65, 2635
- Fritze, H. R. & A. O. Benz, 1981, *ApJ*, 250, 782

- Grall, R. R., W. A. Coles, S. R. Spangler, T. Sakurai, & J. K. Harmon, 1997, JGR102, 263
- Guhuthakurta, M, A. Fludra, S. E. Gibson, D. Biesecker, & R. Fisher, 1999, JGR, 104, 9801
- James, J. C., 1968, Chapter 7 in Radar Astronomy, (eds J. V. Evans & T. Hagfors), McGraw-Hill, New York
- James, J. C., 1970, Solar Phys12, 143
- Kerr, F. J., 1952, Proc. IRE, 40, 660
- Parenti, S., B. J. I. Bromage, G. Poletto, G. Noci, J. C. Raymond, & G. E. Bromage, 2000, A&A, 363, 800
- Pottasch, S. R., 1960, ApJ, 131, 68
- Rodriguez, P., 2000, in Radio Astronomy at Long Wavelengths, AGU Geophysical Monograph 119, 155
- Vanzandt, T.E., & Bowles, K.L., 1960, JGR, 65, 2627